REPORT DOCUMENTATION PAGE

Form Approved
OMB No. 0704-0188

1. REPORT DATE *(DD-MM-YYYY)*	**2. REPORT TYPE**	**3. DATES COVERED** *(From - To)*
05-05-2008	Technical Paper	

4. TITLE AND SUBTITLE

Analytical and Kinetic Modeling of Ablation Process (Preprint)

5a. CONTRACT NUMBER

5b. GRANT NUMBER

5c. PROGRAM ELEMENT NUMBER

6. AUTHOR(S)
L. Pekker, N. Gimelshein, & S. Gimelshein (ERC)

5d. PROJECT NUMBER

5e. TASK NUMBER
50260542

5f. WORK UNIT NUMBER

7. PERFORMING ORGANIZATION NAME(S) AND ADDRESS(ES)

Air Force Research Laboratory (AFMC)
AFRL/RZSA
10 E. Saturn Blvd.
Edwards AFB CA 93524-7680

8. PERFORMING ORGANIZATION REPORT NUMBER

AFRL-RZ-ED-TP-2008-158

9. SPONSORING / MONITORING AGENCY NAME(S) AND ADDRESS(ES)

Air Force Research Laboratory (AFMC)
AFRL/RZS
5 Pollux Drive
Edwards AFB CA 93524-7048

10. SPONSOR/MONITOR'S ACRONYM(S)

11. SPONSOR/MONITOR'S NUMBER(S)
AFRL-RZ-ED-TP-2008-158

12. DISTRIBUTION / AVAILABILITY STATEMENT

Approved for public release; distribution unlimited (PA #08203A).

13. SUPPLEMENTARY NOTES
Submitted for presentation at the 40th AIAA Thermophysics Conference, to be held in Seattle, WA, 23-26 June 2008.

14. ABSTRACT

One of the most important issues in CFD modeling of ablation process is the formulation of boundary conditions at the gas-surface interface. These boundary conditions cannot be obtained without analytical or parametric numerical modeling of the Knudsen layer formed near the evaporating surface. Analytical models are therefore of interest for numerical simulation of ablating flows. Recently Pekker, Keidar, and Cambier developed a new analytical model of the Knudsen layer, which takes into account the temperature gradient in the bulk gas. This model uses a bimodal velocity distribution function which preserves the laws of conservation of mass, momentum, and energy within the Knudsen layer and converges to the Chapman-Enskog velocity distribution function at the outer boundary of the Knudsen layer. The main objective of this work is to provide detailed analysis of the applicability of this analytical model of the Knudsen layer through comparison of results with the numerical solutions of the ES-BGK model kinetic equation and DSMC results.

15. SUBJECT TERMS

16. SECURITY CLASSIFICATION OF:			**17. LIMITATION OF ABSTRACT**	**18. NUMBER OF PAGES**	**19a. NAME OF RESPONSIBLE PERSON**
					Dr. Andrew Ketsdever
a. REPORT	**b. ABSTRACT**	**c. THIS PAGE**	SAR	15	**19b. TELEPHONE NUMBER** *(include area code)*
Unclassified	**Unclassified**	**Unclassified**			N/A

Standard Form 298 (Rev. 8-98)
Prescribed by ANSI Std. 239.18

Analytical and kinetic modeling of ablation process (Preprint)

L. Pekker[1], N. Gimelshein, and S. Gimelshein
ERC Inc., 10 East Saturn Blvd., Edwards AFB, CA 93524

Abstract

One of the most important issues in CFD modeling of ablation process is the formulation of boundary conditions at the gas-surface interface. These boundary conditions cannot be obtained without analytical or parametric numerical modeling of the Knudsen layer formed near the evaporating surface. Analytical models are therefore of interest for numerical simulation of ablating flows. Recently Pekker, Keidar, and Cambier developed a new analytical model of the Knudsen layer, which takes into account the temperature gradient in the bulk gas. This model uses a bimodal velocity distribution function which preserves the laws of conservation of mass, momentum, and energy within the Knudsen layer and converges to the Chapman-Enskog velocity distribution function at the outer boundary of the Knudsen layer. The main objective of this work is to provide detailed analysis of the applicability of this analytical model of the Knudsen layer through comparison of results with the numerical solutions of the ES-BGK model kinetic equation and DSMC results.

[1] Electronic address: leonid.pekker.ctr@edwards.af.mil

I. INTRODUCTION

The first analytical model of the Knudsen layer at an ablating surface was introduced by Hertz and Knudsen [1, 2]. This model assumes no collisions in the Knudsen layer, no heat transfer in the bulk gas, and complete absorption of all incoming molecules at the wall, which corresponds to the condensation coefficient equal to unity. This classical model along with its generalizations has been widely used in CFD modeling. In their recent paper, Bond and Struchtrup [3] have extended the Hertz-Knudsen model to the case of thermal conduction in the bulk gas, considered diffuse and specular reflections of particles, and allowed for non-flat wall-gas interfaces. However, their model still ignores collisions in the Knudsen layer and therefore the law of the conservation of momentum does not hold there. It should be noted that the Hertz-Knudsen assumption of no collisions in the Knudsen layer is not self-consistent, because it assumes no relaxation in the kinetic (Knudsen) layer, although the velocity distribution function at the ablative surface has to relax to the gas bulk (equilibrium) distribution function in the Knudsen layer.

Anisimov [4] was the first to introduce a bimodal velocity distribution function in the Knudsen layer in order to consider the vaporization of a metal surface exposed to laser ablation. In this model, Anisimov used mass, momentum, and energy conservation laws to determine the parameters of his bimodal velocity distribution function, thus accounting for collisions in the Knudsen layer. The assumptions in his model are: (1) the flow velocity at the outer boundary of the Knudsen layer is equal to the speed of sound; (2) the gas temperature in the equilibrium (bulk gas) region outside the Knudsen layer (see Fig. 1) is constant, i.e. there is no conductive heat flux to the ablative surface; and (3) all particles that hit the ablative surface are absorbed by it.

Since then, the Anisimov method has been extended to the cases of half-space evaporation problem [5] and evaporation into dense plasma [6-10], where the flow velocity at the outer boundary of the Knudsen layer was assumed to be smaller than the speed of sound and dependent on the properties of the bulk gas. In all these models the authors still assume no conductive heat flux to the ablative surface and complete absorption of particles by the ablative surface. However, the temperature in the plasma core in [6-9] is much higher than the temperature of the ablative surface and, therefore, the thermal conduction can be significant and has to be included in a Knudsen layer model. Pekker, Keidar, and Cambier [11] used a new bimodal velocity distribution function in the kinetic layer and built a more general Knudsen layer model which takes into account the conductivity of the bulk gas and can therefore be used to model flows with large temperature gradients. This model uses a new bimodal velocity distribution function in the Knudsen layer, which preserves the laws of conservation of mass, momentum, and energy and converges to the Chapman-Enskog velocity distribution function at the outer boundary of the layer. However, as in all other bimodal velocity distribution function models, the condensation coefficient in work [11] was assumed to be equal to unity. Then Pekker [12] extended model [11] to the case of arbitrary condensation coefficient in which he also assumed a constant accommodation coefficient that specifies the fractions of diffuse and specular collisions of incident particles on the ablative surface. This model has allowed the author to obtain gas-surface boundary conditions that can be

used for CFD modeling of ablation processes with thermal conduction and arbitrary condensation and accommodation coefficients.

The ablation process can generally be described by the Boltzmann equation and, therefore can be modeled using methods developed for the solution of this equation, such as the direct simulation Monte Carlo (DSMC) method [13-16]. When the derivation from equilibrium is expected to be small, ablation can also be described by a Bhatnagar-Gross-Krook (BGK) kinetic model equation or by more advanced ellipsoidal statistical BGK (ES-BGK) model [17-19]. In this case, no prior approximation for the gas velocity distribution function in the Knudsen layer is necessary. However, the high computational costs of these methods significantly limit their use. The authors of [5, 14-16, 20] have demonstrated that the models that utilize a bimodal velocity distribution function [4] are in good agreement with DSMC simulations and numerical solutions of BGK equation for the evaporation of a monatomic substance with condensation coefficient equal to unity. However, a thorough verification of the new analytical models of the Knudsen layer [11, 12] through detailed comparison with kinetic modeling and Monte Carlo simulation is needed.

The main objective of this article is to provide detailed analysis of the applicability of Knudsen layer model [11] by comparing its predictions with ES-BGK and DSMC results. To validate model [11] we consider a one-dimensional evaporation/condensation process between two parallel plates for different Knudsen numbers. The analytical model of the evaporation process between ablative and absorbing plates, Fig. 1, including the Knudsen layer model [11] is described in Section II. The description of the ES-BGK and DSMC methods is given in Section III. Numerical results and discussion are presented in Section IV

II. ANALYTICAL MODEL

Knudsen Layer. Figure 1 shows the schematic representation of the problem, were T_A and T_B are the temperatures of the *A*-ablative and *B*-absorbing surfaces, $n_{eq,A}$ and $n_{eq,B}$ are the equilibrium vapor densities of *A* and *B* wall materials at temperatures T_A and T_B, respectively, and L is the distance between the plates. For the sake of simplicity, in the model the condensation coefficient at both surfaces is taken to be unity.

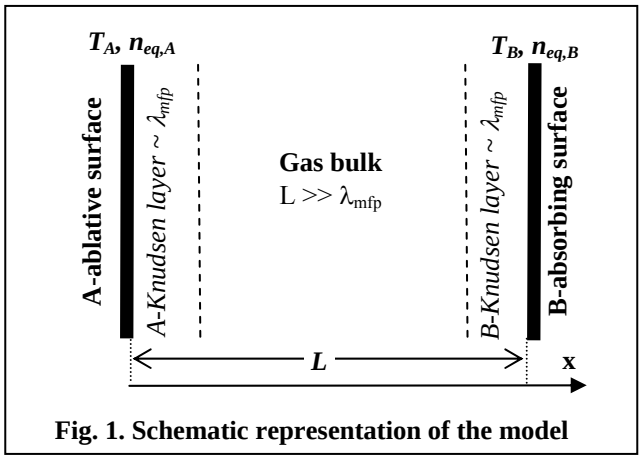

Fig. 1. Schematic representation of the model

It should be stressed that the temperatures of the wall surfaces, equilibrium vapor pressures, molecular mass of vapor molecules and the thermal conductivity of the bulk vapor gas are input parameters of the model. We will choose their values in our calculations only to illustrate the methods and verify the applicability of the analytical Knudsen layer model [11]. Thus, they will not correspond to an actual vaporization process, wall materials, etc.; however, the model certainly can be used for modeling real vaporization processes.

Equations describing the Knudsen layer [11] are

$$\frac{1}{2\cdot\sqrt{\pi}}=\left(\frac{n_{bulk,i}}{n_{eq,i}}\right)\cdot\left(\frac{V_{T_{bulk},i}}{V_{T_i}}\right)\cdot\left[x_i-\frac{\beta_i}{2}\cdot\left[x_i\cdot\mathrm{erfc}(x_i)-\frac{1}{\sqrt{\pi}}\exp\left(-x_i^2\right)\right]\right] \quad , \tag{1}$$

$$\frac{1}{4}=\left(\frac{n_{bulk,i}}{n_{eq,i}}\right)\cdot\left(\frac{V_{T_{bulk},i}}{V_{T_i}}\right)^2\cdot\left[\left(x_i^2+\frac{1}{2}\right)-\frac{\beta_i}{2}\cdot\left[\left(x_i^2+\frac{1}{2}\right)\cdot\mathrm{erfc}(x_i)-\frac{x_i}{\sqrt{\pi}}\cdot\exp\left(-x_i^2\right)\right]\right] \quad , \tag{2}$$

$$\frac{1}{\sqrt{\pi}}=\left(\frac{n_{bulk,i}}{n_{eq,i}}\right)\cdot\left(\frac{V_{T_{bulk},i}}{V_{T_i}}\right)^3\cdot\left[x_i\cdot\left(x_i^2+\frac{5}{2}\right)-\frac{5\cdot\tau_{T_i}}{4}+\frac{\beta_i}{2}\cdot\left[\frac{1}{\sqrt{\pi}}\cdot\left(x_i^2+2\right)\cdot\exp\left(-x_i^2\right)-x_i\cdot\left(\frac{5}{2}+x_i^2\right)\cdot\mathrm{erfc}(x_i)\right]\right] \quad , \tag{3}$$

where

$$x_i=\frac{u_i}{V_{T_i}} \quad , \tag{4}$$

$$V_{T_i}=\sqrt{\frac{2\cdot k\cdot T_i}{m}} \quad , \qquad V_{T_{bulk},i}=\sqrt{\frac{2\cdot k\cdot T_{Tbulk,i}}{m}} \quad . \tag{5}$$

Here, index *i* denotes either surface *A* or surface *B* (see Fig. 1); $V_{T_{bulk},i}$, $n_{T_{bulk},i}$, and u_i are the thermal velocity, number density, and directed vapor velocity of the vapor at the outer boundary of the *i*-th Knudsen layer, Fig. 2; V_{T_i} is the thermal velocity of vapor corresponding to the wall temperature T_i; m is the mass of the vapor molecule; x_i is the ratio of the bulk gas velocity to the thermal velocity at the outer boundary of the *i*-th Knudsen layer, Fig. 2. Equations (1) – (3) correspond to the laws of mass, momentum, and energy conservation, respectively, inside the Knudsen layer [11]. In Eq. (3) τ_{T_i} is a thermal conduction parameter,

$$\tau_{T_i} = \frac{8 \cdot \chi_{gas}}{5 \cdot n_{bulk,i} \cdot k \cdot V_{T_{bulk,i}}^2} \cdot \left. \frac{dV_{T_{bulk,i}}}{dz} \right|_{KL} = \frac{\lambda_{mfp}}{\delta x_T} << 1 \quad , \tag{6}$$

where

$$\lambda_{mfp} = \frac{4 \cdot \chi_{gas}}{5 \cdot n_{bulk,i} \cdot k \cdot V_{T_{bulk,i}}} \quad , \tag{7}$$

$$\delta x_T = \frac{1}{T_{bulk,i}} \cdot \left. \frac{d(T_{bulk,i})}{dz} \right|_{KL} \quad . \tag{8}$$

are the gas mean-free-path and characteristic gradient length at the outer boundary of the kinetic layer, respectively, and χ_{gas} is the thermal conductivity of the bulk gas. Condition (6), $\lambda_{mfp} << \delta x_T$, is needed for the Chapman-Enskog expansion method to be valid [31] and is used in the derivation of Eq. (3) [11]. The parameter β in Eqs. (1) – (3) is an unknown variable that must be obtained in the solution; essentially, it represents nonequilibrium effects caused by collisions in the Knudsen layer [4]. It is worth noting that the case of $u_i > 0$ corresponds to the ablation process, Fig. 2, while the case of $u_i < 0$ corresponds to absorption process.

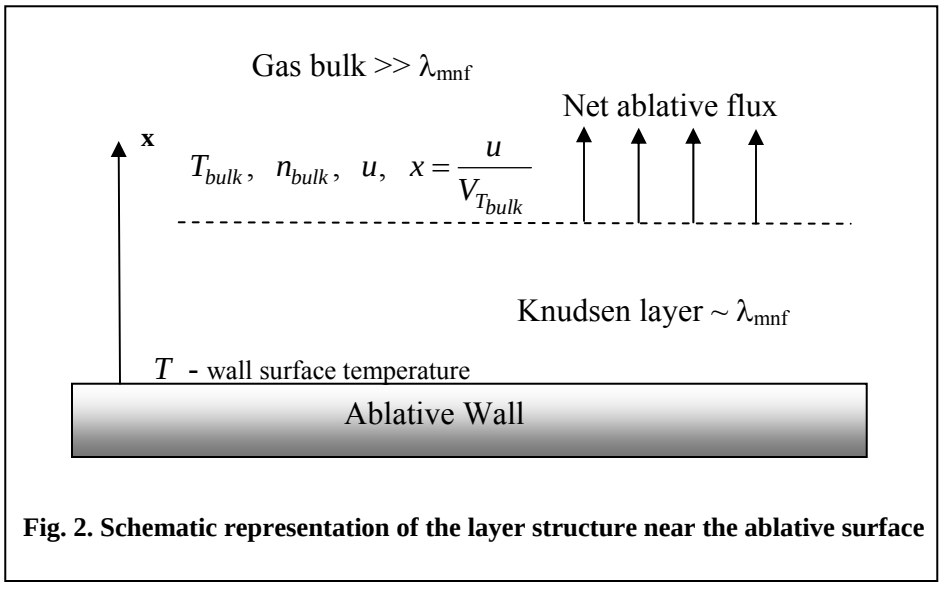

Fig. 2. Schematic representation of the layer structure near the ablative surface

Thus, if we know two parameters, for example x_A and τ_{T_a}, the system of Eqs. (1) – (3) is complete (the wall temperature T_A and equilibrium vapor number density $n_{eq,A}$ are assumed to be known – they are input parameters of the model) and $V_{T_{bulk,A}}$, $n_{bulk,A}$ and β can be calculated, then using Eqs. (4) and (5) we can calculate $T_{bulk,A}$ and u_A.

Gas Bulk. Now let us consider the gas bulk region. In this region, Fig. 1, the mass flux, momentum flux, and energy flux equations [21] are

$$M_x = m \cdot n_{bulk} \cdot u_{bulk} \quad , \tag{9}$$

$$P_x = m \cdot n_{bulk} \cdot \left(u_{bulk}^2 + \frac{V_{T_{bulk}}^2}{2} \right) \quad , \tag{10}$$

$$E_x = -\chi_{gas} \cdot \frac{dT_{bulk}(z)}{dz} + m \cdot n_{bulk} \cdot u_{bulk} \cdot \left[\frac{5}{4} \cdot V_{T_{bulk}}^2 + \frac{u_{bulk}^2}{2} \right] \tag{11}$$

where

$$T_{bulk} = \frac{m \cdot V_{T_{bulk}}^2}{2 \cdot k} \tag{12}$$

is the gas bulk temperature and χ_{gas} is the thermal conductivity of the bulk gas. Obviously, in general the gas bulk density, n_{bulk}, the bulk gas temperature, T_{bulk}, and the bulk gas directed velocity, u_{bulk}, are dependent on the *x*-coordinate, Fig. 1. In the stationary case, considered in this paper, the mass, momentum, and energy fluxes M_x, P_x, and E_x are conserved inside the bulk gas region. The boundary conditions at the outer boundaries of the *A*- and *B*-Knudsen layers can be written as

$$n_{bulk}(x=0) = n_{bulk,A}, \quad V_{T\,bulk}(x=0) = V_{T\,bulk,A}, \quad u_{bulk}(x=0) = u_{bulk,A} \quad , \tag{13}$$

$$n_{bulk}(x=0) = n_{bulk,B}, \quad V_{T\,bulk}(x=0) = V_{T\,bulk,B}, \quad u_{bulk}(x=0) = u_{bulk,B} \quad . \tag{14}$$

It is worth noting that since the velocity distribution function in the Knudsen layer [11] converges to the Chapman-Enskog velocity distribution function at the outer boundary of the Knudsen layer, Fig. 2, the boundary conditions (13) and (14) automatically preserve the fluxes of mass, momentum, and energy within the entire region between the two walls, including both Knudsen layers.

Expressing u_{bulk}, T_{bulk} and n_{bulk} via $V_{T_{bulk}}$, E_x, M_x, and P_x, Eqs. (9) – (13), we obtain

$$E_x = M_x \cdot \left(\frac{1}{2} \cdot \left[\frac{V_{T_{bulk}}^2 \cdot M_x}{P_x + \sqrt{P_x^2 - 2 \cdot V_{T_{bulk}}^2 \cdot M_x^2}} \right]^2 + \frac{5}{4} \cdot V_{T_{bulk}}^2 \right) - \frac{\chi_{gas} \cdot m}{k} \cdot V_{T_{bulk}} \cdot \frac{dV_{T_{bulk}}}{dz} \quad , \tag{15}$$

$$u_{bulk} = \frac{V_{T_{bulk}}^2 \cdot M_x}{P_x + \sqrt{P_x^2 - 2 \cdot V_{T_{bulk}}^2 \cdot M_x^2}} \quad , \tag{16}$$

$$n_{bulk} = \frac{\left(P_x + \sqrt{P_x^2 - 2 \cdot V_{T_{bulk}}^2 \cdot M_x^2} \right)}{m \cdot V_{T_{bulk}}^2} \quad . \tag{17}$$

Thus, by numerically solving Eq. (15) for $V_{T_{bulk}}$ for given E_x, M_x, and P_x, we can calculate the gas thermal velocity distribution vs. the *x*-coordinate in the gas bulk region, and then, by using Eqs. (12), (16) and (17) we obtain the distributions of T_{bulk}, u_{bulk}, n_{bulk}, and finally calculate the thermal conduction parameter τ_T, Eq. (6), at the outer boundary of the Knudsen layer.

Algorithm. Now let us describe a possible algorithm for calculating the gas bulk distributions and parameters of the Knudsen layers for given wall surfaces temperatures and corresponding equilibrium vapor number densities.

1. Assume initial values of x_A and τ_{T_a}.
2. Calculate all parameters of the *A*-Knudsen layer as described in the Knudsen Layer Section.
3. Use Eqs. (6) – (8) to calculate mass, momentum, and energy fluxes at the outer boundary of the Knudsen layer, where and the temperature gradient can be determined from Eqs. (6) – (8).
4. Integrate Eq. (15) to obtain $V_{T\,bulk,B}$, the gas thermal velocity at the outer boundary of the *B*-Knudsen layer.
5. Use Eqs. (16), (17) and (12), and then (6) – (8) to obtain $u_{bulk,B}$, $T_{bulk,B}$, $n_{bulk,B}$, and τ_{T_B}.

6. Use Eq. (4) to calculate x_B.

7. Use Eqs. (1) – (3) to calculate β_B, wall temperature T_B^*, and equilibrium vapor density $n_{eq,B}^*$.

8. If the calculated T_B^* and $n_{eq,B}^*$ are not equal to given wall temperature T_B and equilibrium number density $n_{eq,B}$ we have to go Step 1 and change x_A and τ_{T_a}.

In this work we have used the Newton-Raphson method to iterate the values of x_A and τ_{T_a}. The mass of vapor molecules and gas thermal conductivity in the bulk region have been chosen as

$$m = 7.7467 \text{ kg} \quad \text{and} \quad \chi_{gas} = 0.10022 \cdot (T/273)^{3/4} \text{ W/(m·K)} \quad , \tag{18}$$

and the input parameters of the runs are shown in Table 1. Since there are two Knudsen layer, Fig. 1, the Knudsen in the Table 1 have been taken as $2 \cdot \lambda_{mfp} / L$, where λ_{mfp} has been calculated using Eq. (7) for $T = 300\ K$.

Table 1. Input parameters for modeling

	$L[m]$	$T_A[K]$	$n_{eq,A}[m^{-3}]$	$T_B[K]$	$n_{eq,B}[m^{-3}]$	$\lambda_{mfp}[m]$	$2 \cdot \lambda_{mfp} / L$
1	5.24e-4	300	4.59e+22	413.24	3.06+22	1.31e-4	0.5
2	1.31e-3	300	4.59e+22	413.24	3.06+22	1.31e-4	0.2
3	2.62e-3	300	4.59e+22	413.24	3.06+22	1.31e-4	0.1
4	5.24e-3	300	4.59e+22	413.24	3.06+22	1.31e-4	0.05
5	1.31e-2	300	4.59e+22	413.24	3.06+22	1.31e-4	0.02
6	2.62e-2	300	4.59e+22	413.24	3.06+22	1.31e-4	0.01

We have divided the distance between the plates, Fig. 1, into 10^4 equal-length intervals to numerically solve Eq. (15) and used 10^4 iterations in Newton-Raphson method to obtain x_A and τ_{T_a}. The code was written in Java; each run took a few minutes on a PC with a Pentium 4 processor. Increasing the space steps by a factor of two (i.e., using 5×10^3 intervals) led to relative errors in x_A and τ_{T_a} of $7\cdot10^{-6}$ and $3.5\cdot10^{-4}$, respectively, for $L = 2.62\cdot10^{-2}$ m; they monotonically decrease with L down to $7\cdot10^{-7}$ for $L = 5.24\cdot10^{-4}$ m.

III. KINETIC APPROACHES

Two kinetic approaches have been used in this work for the validation of the Pekker-Keidar-Cambier analytical model [11] of the Knudsen layer, the DSMC method and the solution of the ES-BGK model kinetic equation.

In the DSMC calculations we have used the DSMC-based SMILE computational solver (details on the tool may be found elsewhere [22]) with a uniform spatial grid for modeling collisions and macro parameters. The one-dimensional problem shown in Fig. 1 was modeled using the 2D module of SMILE with a single row of cells bounded by specularly reflected walls in the transversal direction, and the longitudinal walls at *A*- and *B*-surfaces, Fig. 1, absorbing all incident particles. The majorant frequency scheme [23] was employed for modeling molecular collisions. The variable hard sphere (VHS) model [24] was used for intermolecular interactions, with the reference particle diameter of 2.8 A at a reference temperature of 273K, and the exponent in the viscosity-temperature dependence of 0.75. The DSMC modeling was conducted for $L = 5.24 \cdot 10^{-4}$ and $5.24 \cdot 10^{-3}$ m for which the grid and number of molecules convergence were obtained. The results shown below were obtained for 4,000 cells and about 4 million molecules, and ran over 1 million time-steps that took approximately 300 CPH. The numerical error is estimated to be about 1 percent.

For solving ES-BGK equation, we have used a finite volume solver SMOKE developed at ERC Inc. SMOKE is a parallel code based on conservative numerical scheme developed by Mieussens [24]. A second order spatial discretization is used along with implicit time integration. The boundary conditions at *A*- and *B*-surfaces were set to simulate the condensation coefficient of unity, and the distribution function in the ghost cells was equilibrium with the corresponding parameters specified in Table 1. The viscosity-temperature dependence was the same as in the DSMC modeling. The spatial grid convergence was achieved increasing the number of nodes from 200 to 2,000 with non-uniform cell sized to account for stronger gradients near the walls. The convergence on the velocity grid was also studied with the number of bins in (x, y, z) directions ranging from (10, 10, 10) to (30, 20, 20). The longest run for L = 2.62e-2 m, Table 1, took approximately 15 CPH. The numerical error is estimated to be less then 1.5 percents.

IV. NUMERICAL RESULTS AND DISCUSSION

Let us first compare the distributions of gas density and temperature obtained using the two kinetic approaches with the density and temperature distributions obtained by the analytical model. The results for the most rarefied case, $L = 5.24 \cdot 10^{-4}$ m and $Kn = 0.5$ (Table 1) are presented in Fig. 3. As one can see an agreement between the DSMC and ES-BGK solutions seems very reasonable almost everywhere accept the region closed to the wall. However, the density and temperature distributions obtained by the analytical approach are far-off from the kinetic distributions. This observation has a simple explanation. In all analytical models of the Knudsen layer [1-12], the Knudsen layer is considered as a zero-dimensional interface between the wall and gas bulk. However, in this situation, where the thickness of the Knudsen layer is about the gap between the walls, Fig. 3, this approximation is rather not valid. The differences between the kinetic and

analytical distributions of macroparameters decrease as the Knudsen number decreases as shown in Fig. 4, where $L = 5.24 \cdot 10^{-3}$ m and $Kn = 0.05$ (Table 1).

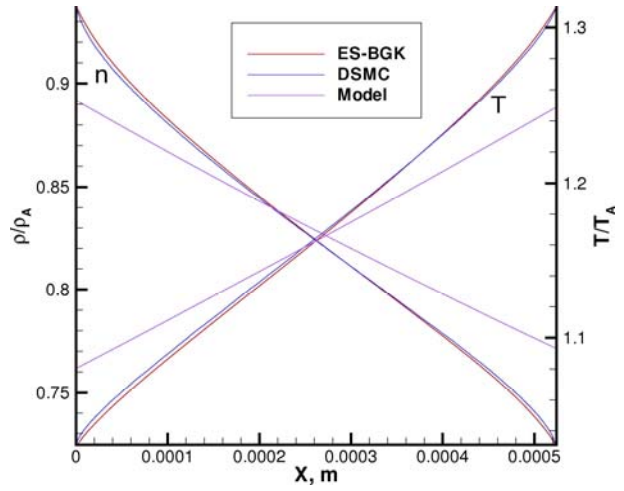

Fig. 3. Profiles of density and temperature between ablative plates for two kinetic approaches and the analytic model for $L = 5.24 \cdot 10^{-4}$ m

As one can see, the differences between the profiles of macroparameters obtained by kinetic modeling and using analytical approximations are much smaller here than for the case of $L = 5.24 \cdot 10^{-3}$ shown in Fig. 3, but still noticeable. These differences again can be explained by neglecting the thickness of the Knudsen layer in the analytical model [11].

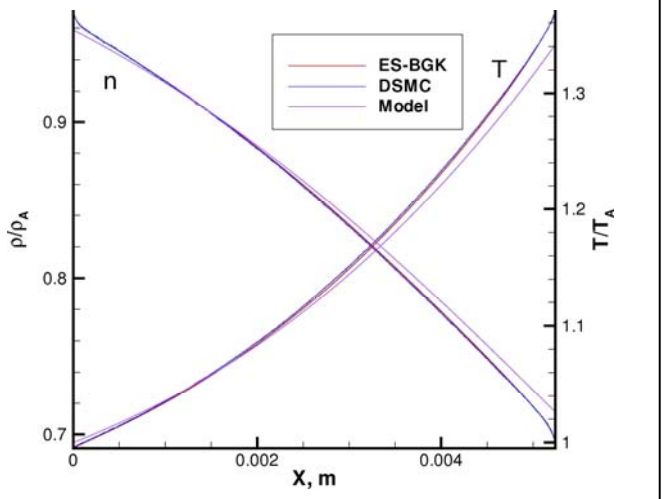

Fig. 4. Profiles of density and temperature between ablative plates for two kinetic approaches and the analytic model for $L = 5.24 \cdot 10^{-3}$ m

The effect of thermal non-equilibrium in the ES-BGK solution is illustrated in Fig. 5, where the computed distribution function of longitudinal velocity is compared to the corresponding Maxwellian distribution function with the local temperature and velocity, for $L = 5.24 \cdot 10^{-4}$ at $x = L/2$. The ratio of the ES-BGK to the Maxwellian distribution is also shown in Fig. 5. In the central region (the velocity is close to the averaged longitudinal velocity, u_{bulk} in Eq. (9)), the deviation of the computed function from the Maxwellian distribution is relatively small, while for the tails of the distribution functions it reaches a factor of two and more.

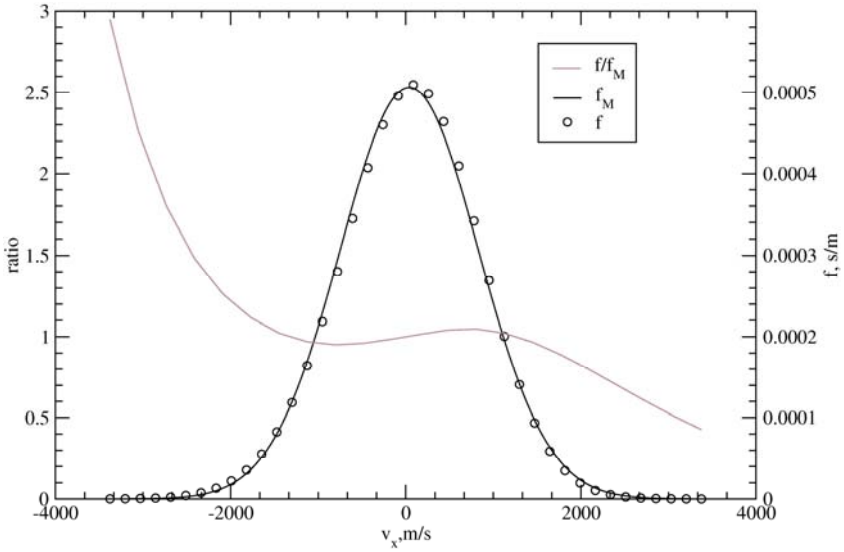

Fig. 5. Longitudinal velocity distribution functions in the center of the computational domain $L = 5.24 \cdot 10^{-4}$ m

The most important properties that the analytical model is expected to provide are the mass, momentum, and energy fluxes from cold to hot ablative surfaces. Comparison of the fluxes computed using different approaches is given in Table 2. With an increase in the distance between the plates the mass fluxes decrease while the energy fluxes increase for all three models. The decrease in the mass flux is associated with lower flow velocities in the longitudinal direction, Eq. (9), and the increase in the energy flux is related to smaller impact of reverse thermal fluxes directed from hot to cold surface, Eq. (11). The momentum flux practically does not change with the distance between plates, because it is related mostly to the gas bulk pressure, Eq. (10), which in turn is determined by the outflow conditions on the plates (equilibrium vapor pressures) and not by the distance between the plates.

Table 2. Mass, energy, and momentum fluxes

		Analytical			*ES-BGK*			*DCMS*	
L	$2\cdot\lambda_{mnf}$	M_x	P_x	E_x	M_x	P_x	E_x	M_x	E_x
m	m	$kg\cdot m^{-2}\cdot s^{-1}$	$kg\cdot m^{-2}\cdot s^{-2}$	$W\cdot m^{-2}$	$kg\cdot m^{-2}\cdot s^{-1}$	$kg\cdot m^{-2}\cdot s^{-2}$	$W\cdot m^{-2}$	$kg\cdot m^{-2}\cdot s^{-1}$	$W\cdot m^{-2}$
5.24e-4	2.62e-4	1.043e-2	1.8252e+2	4.585e+3	1.193e-2	1.8253e+2	2.836e+3	1.178e-2	2.638e+3
1.31e-3	2.62e-4	8.910e-3	1.8245e+2	6.755e+3	9.475e-3	1.8246e+2	6.280e+3		
2.62e-3	2.62e-4	7.994e-3	1.8238e+2	8.060e+3	8.249e-3	1.8240e+2	7.978e+3		
5.24e-3	2.62e-4	7.412e-3	1.8234e+2	8.887e+3	7.553e-3	1.8234e+2	8.955e+3	7.380e-3	8.832e+3
1.31e-2	2.62e-4	7.106e-3	1.8231e+2	9.322e+3	7.198e-3	1.8232e+2	9.433e+3		
2.62e-2	2.62e-4	7.075e-3	1.8231e+2	9.366e+3	7.169e-3	1.8231e+2	9.485e+3		

The relative differences between analytical, ES-BGK, and DSMC results calculated by the following formula,

$$\hat{M}_{x,\alpha} = 100 \cdot \frac{(M_{x,BGK} - M_{x,\alpha})}{M_{x,ES-BGK}}, \quad \hat{E}_{x,\alpha} = 100 \cdot \frac{(E_{x,BGK} - E_{x,\alpha})}{E_{x,ES-BGK}} \tag{19}$$

where index α denotes either analytical or DSMC solution, are shown in Table 3. The differences between the analytical and kinetic solutions for $L \geq 5.24\cdot10^{-3}$ are within the numerical error of the computations. For the smaller L (larger Knudsen numbers), there is a noticeable differences between the kinetic solutions and analytical approach. The differences in the energy fluxes $\hat{E}_{x,DSMS}$ and $\hat{E}_{x,analyt}$ reach about 7% and 61%, respectively, for $L = 5.24\cdot10^{-4}$. Such differences are expected because the ES-BGK model is a simplification of the Boltzmann equation, and the analytical approximation assumes a small deviation from the Maxwellian distribution function (small Knudsen numbers). The ES-BGK model works better for relatively large Knudsen numbers than the analytical approximation, Table 3. However, for $L = 1.31\cdot10^{-3}$ the differences in mass and energy fluxes obtained by ES-BGK and analytical approaches are about 6% and -7.6%, respectively.

Thus, we may conclude that the numerical results presented in this paper clearly show that the Pekker-Keidar-Cambier analytical model [11] of the Knudsen layer gives the reasonable approximations for mass, energy, and momentum fluxes for Knudsen number smaller than 0.2.

Table 3. Relative differences between analytical, ES-BGK, and DSMC results

L	$2 \cdot \lambda_{mfp}$	$\hat{M}_{x,analyt}$	$\hat{E}_{x,analyt}$	$\hat{M}_{x,DSMC}$	$\hat{E}_{x,DSMC}$
m	m	%	%	%	%
5.24e-4	2.62e-4	12.55	-61.65	1.25	6.99
1.31e-3	2.62e-4	5.96	-7.56		
2.62e-3	2.62e-4	3.09	-1.02		
5.24e-3	2.62e-4	1.87	0.76	2.29	2.49
1.31e-2	2.62e-4	1.28	1.17		
2.62e-2	2.62e-4	1.31	1.26		

References

[1] H. Hertz, Ann. Phys. (Leipzig) **17**, 177 (1882).

[2] M. Knudsen, Ann. Phys. (Leipzig) **47**, 697 (1915).

[3] M. Bond and H. Struchtrup, Phys. Rev. E **70,** 061605 (2004).

[4] S. I. Anisimov, Sov. Phys. JETP **27,** 182 (1968).

[5] T. Ytrehus, Rarefied Gas Dyn. **51**, 1197 (1977).

[6] I. I. Beilis, IEEE Trans. Plasma Sci. **13,** 288 (1985).

[7] I. I. Beilis, "*Theoretical Modeling of Cathode Spot Phenomena*" in book "*Vacuum Arc Science and Technology*", R. L. Boxman, P. Martin, D. Sanders (Editors) (Park Ridge, NJ, Noyes Publications, 1995).

[8] M. Keidar, J. Fan, I. D. Boyd, and I. I. Beilis, J. Appl. Phys. **89,** 3095 (2001).

[9] M. Keidar, I. D. Boyd and I. I. Beilis, J. Phys. D: Appl. Phys. **34,** 1675 (2001).

[10] M. Keidar, I. D. Boyd and I. I. Beilis, J. Appl. Phys. **96,** 5420 (2004).

[11] L. Pekker, M. Keidar, J.-L. Cambier, J. Appl. Phys. **103**, 034906 (2008).

[12] L. Pekker, 40th AIAA Thermophysics Conference, 23-26 June 2008, Seattle, WA (2008).

[13] G. A. Bird, "*Molecular Gas Dynamics and the Direct Simulation of Gas Flow, Clarendon Press*", Oxford (1994).

[14] D. Sibold, H.M. Urbassek, Phys. Rev. **A. 43** 6722 (1991).

[15] D. Sibold, H.M. Urbassek, Phys. Fluids A., **5**, 243 (1993).

[16] A. A. Morozov, Applied Phys. A **79**, 997 (2004).

[17] P. L. Bhatnagar, E. P. Gross, M. A. Krook, Phys. Rev. **94**, 511 (1954).

[18] L. H. Holway, Rarefied Gas Dynamics **1**, 193 (1966).

[19] I. N. Shishkova and S.S. Sazhin, J. Comp. Phys., **218**, 635 (2006).

[20] J.W. Rose, International Journal of Heat and Mass Transfer **43**, 3869 (2000).

[21] W. G. Vincenti and C. H. Kruger, Jr., Introduction to Physical Gas Dynamic (Krieger, Malabar, FL. (1975).

[22] M.S. Ivanov, G.N. Markelov, S.F. Gimelshein, AIAA Paper 98-2669.

[23] M.S. Ivanov, S.V. Rogasinsky, Sov. J. Numer. Anal. Math. Modeling **2**(6), 453 (1998).

[24] G. A. Bird, *Monte-Carlo simulation in an engineering context*, Rarefied Gas Dynamics **74**, 239 (1981), ed. S Fisher, Progress in Astronautics and Aeronautics

[25] L. Mieussens, Journal of Computational Physics **162**, 429 (2000).